Acta Geochim (2026) 45:111–131
https://doi.org/10.1007/s11631-025-00787-6

ORIGINAL ARTICLE

Dissolution kinetics of a low-grade oxide-sulfide copper ore with high silica content: Laboratory studies and statistical modeling

Hiva Farhadi[1,2] · Faramarz Doulati Ardejani[1,2] · Sied Ziaedin Shafaei Tonkaboni[1] · Soroush Maghsoudy[1,2] · Roya Kafi[3] · Helia Tafakori[1,2] · Christoph Butscher[4] · Reza Taherdangkoo[4]

Received: 4 February 2025 / Revised: 31 March 2025 / Accepted: 13 May 2025 / Published online: 15 June 2025

Abstract In this study, copper extraction from low-grade oxide-sulfide ores was investigated using a leaching method combined with response surface methodology (RSM) to optimize operational conditions and assess leaching kinetics. Given copper's extensive industrial applications, sustainable recovery from low-grade ores is critical. Five key parameters-acid concentration, leaching time, particle size, temperature, and solids percentage-were identified as major influences on copper recovery. The results revealed that leaching time and solids percentage, along with interactions between temperature-time and temperature-solids percentage, had the most significant effects. Optimal conditions for 80% copper recovery while minimizing iron recovery below 3% included an acid concentration of 1.21 mol L^{-1}, a leaching time of 108 min, a particle size of 438 μm, a temperature of 45 °C, and a solids percentage of 18.2%. Leaching kinetics were analyzed using shrinking core models, with the Dickinson model best describing the process, showing an activation energy of 32.63 kJ mol^{-1}, indicative of mixed diffusion and chemical reaction control. The final kinetic model effectively predicted the influence of key parameters. These findings highlight the importance of optimizing process variables and selecting suitable kinetic models to enhance extraction efficiency, reduce costs, and improve sustainability in copper recovery.

Keywords Oxide-sulfide ore · Response surface methodology · Kinetic analysis · Miduk copper mine · Shrinking core model · Copper leaching

1 Introduction

The escalating industrial and market demand for raw materials has intensified efforts to discover and extract various metals. Among these, copper stands out as a base metal with extensive applications, rendering it both strategic and vital (Schlesinger et al. 2021; Mahmoudi Kouhi et al. 2024). In nature, copper associates with nearly all elements of the periodic table, forming a diverse array

✉ Reza Taherdangkoo
reza.taherdangkoo@ifgt.tu-freiberg.de

Hiva Farhadi
h.farhadi@ut.ac.ir

Faramarz Doulati Ardejani
fdoulati@ut.ac.ir

Sied Ziaedin Shafaei Tonkaboni
zshafaie@ut.ac.ir

Soroush Maghsoudy
s.maghsoudy@ut.ac.ir

Roya Kafi
kafi_roya@nicico.com

Helia Tafakori
heliatafakori@gmail.com

Christoph Butscher
christoph.butscher@ifgt.tu-freiberg.de

[1] School of Mining, College of Engineering, University of Tehran, Tehran, Tehran 100190, Iran

[2] Mine Environment and Hydrogeology Research Laboratory (MEHR Lab.), University of Tehran, Tehran, Tehran 10587, Iran

[3] Research and Development Unit, Miduk Copper Complex, Kerman 76341, Iran

[4] Institute of Geotechnics, TU Bergakademie Freiberg, Gustav-Zeuner-Str. 1, Freiberg 09599, Germany

of minerals, including carbonates, silicates, hydroxides, oxides, chlorides, sulfates, phosphates, and sulfides. This versatility results in a wide range of copper-bearing resources within the Earth's crust. To date, over 150 copper minerals have been identified, yet fewer than 17 hold significant commercial value (Gupta and Mukherjee 2017; Davenport et al. 2002).

The main copper resources include sulfide and oxide minerals, among which chalcopyrite ($CuFeS_2$), covellite (CuS), chalcocite (Cu_2S), malachite [$Cu_2(OH)_2CO_3$], chrysocolla [$(Cu,Al)_2H_2Si_2O_5(OH)_4$. nH_2O], azurite ($Cu3(OH)_2(CO_3)_2$), and bornite (Cu_5FeS_4) are among the most important (Gupta and Mukherjee 2017; Schlesinger et al. 2021). In recent years, increasing copper demand, driven by economic growth, has led to a depletion of high-grade sulfide and oxide deposits. Consequently, secondary sources, including low-grade ores and flotation tailings, have garnered significant attention as a serious alternative for meeting copper requirements (Habashi 1980; Han et al. 2018; Li et al. 2018).

Until about five decades ago, the principal route for producing metallic copper relied on processing sulfide concentrates via pyrometallurgical techniques (Davenport et al. 2002; Schlesinger et al. 2021). This approach still accounts for approximately 80% of global copper production (Free 2013). However, in recent decades, advancements in solvent extraction (SX) and electrowinning (EW), coupled with improvements in concentrating pregnant leach solutions (PLS) derived from oxide, low-grade sulfide, and mixed oxide–sulfide deposits, have enabled alternative copper production methods (Mahmoudi Kouhi et al. 2024; Wadsworth and Sohn 1979; Gupta and Mukherjee 2017).

A key development in the copper industry is the shift toward hydrometallurgical processes, which facilitate the use of small and low-grade oxide–sulfide copper deposits while overcoming limitations of pyrometallurgical routes such as high capital expenditure, substantial environmental concerns, and elevated energy demands (Watling 2006; Schlesinger et al. 2021). The increasing prominence of hydrometallurgy largely stems from its enhanced environmental compatibility, reduced energy consumption, and the introduction of more selective extractants, ion-exchange resins, as well as bioleaching techniques employing specialized microorganisms (Rawlings and Johnson 2007; Watling 2006). Recent data shows that hydrometallurgical methods have significantly boosted copper and base metal production. Forecasts predict continued growth in hydrometallurgical output, driven by factors like the depletion of high-grade copper reserves, rising copper prices, and increased demand. As a result, the focus has shifted towards processing low-grade ores, with hydrometallurgical and bio-hydrometallurgical methods becoming increasingly important (Liu et al. 2016; Li et al. 2013; Katal et al. 2020).

Leaching, as the initial step in hydrometallurgy (Schlesinger et al. 2021), plays a pivotal role in extracting metals from mineral deposits (Davenport et al. 2002) by employing suitable chemical reagents (Li et al. 2013 that transfer the metals from the solid phase into the liquid phase (Watling 2006). Owing to its high flexibility and suitability for low-grade resources or secondary materials (Free 2013), Leaching is a primary method for metal extraction. The choice of reagent (acidic or alkaline) and operational conditions directly affect the process's efficiency and performance (Antonijević et al. 2008).

The primary objective at this stage is to establish conditions that enable the complete dissolution of the target metal, thus preparing it for subsequent processing steps (Habashi 1980; Schlesinger et al. 2021). In this context, studying the leaching kinetics is critical for gaining a deeper understanding of both reaction mechanisms and mass transfer processes (Levenspiel 1998). Kinetic analyses are indispensable for examining the reaction rates and determining factors that influence metal recovery (Free 2013). By evaluating these rates, researchers and engineers can identify optimal strategies for extracting metals from low-grade materials. These strategies not only help reduce operational costs and increase economic efficiency but also contribute to environmental sustainability by lowering the consumption of resources, energy, and chemicals, as well as reducing waste production and environmental pollution (Davenport et al. 2002). In metal extraction processes, a thorough study of reaction kinetics from laboratory to industrial scales is of great importance. By better understanding the reaction mechanisms, parameters such as reaction time, temperature, and reagent concentration can be optimized, leading to improved process efficiency and reduced operational costs (Habashi 1980). Furthermore, kinetic models such as the shrinking core model provide a robust framework for pinpointing specific dissolution mechanisms, which in turn aids in designing systems with improved process control and lower environmental impacts (Haghighi et al. 2013; Crundwell 2014).

Many recent studies have examined efficient recovery and dissolution kinetics of copper from low-grade and secondary sources using various reagents. Sulfuric acid leaching remains one of the most common and cost-effective methods, given its operational simplicity and low production expenses (Tanda et al. 2019; Sun et al. 2009). For instance, Bingol and Canbazoğlu (2004) described malachite dissolution in sulfuric acid as a two-stage process with an activation energy of 1.3 kJ mol^{-1}, indicating diffusion control. Increasing the temperature from 25 to 80 °C raised copper recovery from 94% to 98%, requiring acid concentrations above 1.02 mol L^{-1} for complete dissolution.

Chen et al. (2014) reported high recovery of multiple metals from low-grade copper sulfide tailings, while Bai et al. (2018) applied the shrinking core model to cuprite

dissolution, achieving over 92% copper recovery. Tanda et al. (2019) found product-layer diffusion dominant in chalcopyrite leaching with alkaline glycine solutions, and (Ajiboye et al. 2019) demonstrated nearly complete dissolution of copper and zinc from e-waste. Recent work by Apua et al. (2013) and Bayati et al. (2018) similarly confirmed that Optimizing parameters like temperature, time, and acid concentration boosts extraction efficiency, with kinetic modeling identifying rate-controlling mechanisms.

The recovery of copper from oxide–sulfide ores poses considerable difficulties due to their intricate chemical composition and crystalline structure (Davenport et al. 2002). Such complexity makes dissolution processes highly sensitive to a range of parameters, complicating the identification of universal optimal conditions and often elevating operational costs (Montgomery 2001; Taherdangkoo et al. 2022). Moreover, synergistic effects among variables like temperature, acid concentration, and agitation speed further influence the dissolution rate, emphasizing the need for well-structured experimental designs (Montgomery 2001).

Response Surface Methodology (RSM) has proven to be a powerful approach for optimizing multifactor processes such as copper recovery. By applying mathematical modeling to elucidate how different variables interact, RSM can minimize the number of experimental runs while providing precise estimates of key process parameters. A central element of this methodology is the Central Composite Design (CCD), which not only organizes experiments efficiently but also allows for the evaluation of linear, nonlinear, and interaction effects to pinpoint optimal conditions (Montgomery 2001). These models help identify optimal conditions where metal recovery is maximized while the consumption of resources, energy, and chemicals is optimized. By managing and optimizing parameters such as acid concentration, reaction time, and particle size, waste production is reduced, and environmental impacts such as pollution and the generation of acid solutions are minimized. This optimization leads to reduced energy and natural resource consumption, ultimately making the process sustainable and economically viable (Mohanraj et al. 2022; Javed et al. 2018).

This study aims to investigate, optimize, and analyze the extraction and recovery of copper from oxide–sulfide ore. Specifically, the copper dissolution behavior of a sample ore is examined to provide insight into the mechanisms governing this process. To optimize copper recovery, RSM with CCD was employed, enabling the identification of optimal operating conditions. Additionally, process modeling was conducted using the shrinking core model, offering a detailed analysis of the kinetics and dissolution mechanisms of copper, as well as the factors influencing the process.

2 Materials and methods

2.1 Materials

In this study, 200 kg of ore was sourced from the heap leaching operation at the Miduk Copper Mine in Kerman Province. After crushing, the material was classified into five particle-size fractions: 75 µm, 100 µm, 400 µm, 700 µm, and 1000 µm. Each fraction was thoroughly homogenized and subdivided using a riffle splitter. Subsequently, 200 g of the sample (used as a reference) was sent to the laboratory for XRF, XRD, and ICP-MS analyses. The main and

Table 1 XRF analysis of the reference sample

Compound	SiO_2	Al_2O_3	BaO	CaO	Fe_2O_3	K_2O	MgO	Na_2O
Content (%)	51.19	16.15	0.05	0.45	8.07	3.40	1.61	0.45
Compound	P_2O_5	SO_3	TiO_2	SrO	CuO	LOI		
Content (%)	0.27	9.98	0.93	<0.01	0.21	7.24		

Table 2 XRD analysis of the copper ore sample

Phase (%)	Chemical formula	Mineral name (Solid Phase)
44	SiO_2	Quartz
5	$NaAlSi_3O_8$	Albite
2	$KAlSi_3O_8$	Potassium Feldspar
8	FeS_2	Pyrite
6	$(Mg,Fe)_6(Si,Al)_4O_{10}(OH)_8$	Chlorite
29	$KAl_2Si_3AlO_{10}(OH)_2$	Muscovite–Illite
5	$Al_2Si_2O_5(OH)_4$	Kaolinite
1	$CaCO_3$	Calcite

Table 3 ICP-MS analysis of the reference copper ore sample

Element	Ag	Al	As	Ba	Ca	Cd	Cr	Cu	Fe	K
Content (ppm)	0.5	84,699	44.2	408	3529	0.2	95	4538	47,839	24,968

Element	Mo	Mg	Na	Ni	P	Pb	Ti	Zn
Content (ppm)	3.7	7852	3208	27	1242	129	3394	66

trace element composition (XRF) is listed in Table 1, the mineralogical composition (XRD) is shown in Table 2, and concentrations of key elements and heavy metals (ICP-MS) are provided in Table 3.

Based on XRF and XRD results, the sample contains a high silica (quartz) content with low calcite. This mineralogical profile is advantageous for acid leaching since silicate minerals are generally inert, reducing the acid consumption that would otherwise be higher in the presence of carbonate minerals. The sample also contains approximately 8% pyrite, which could influence oxidation reactions under acidic conditions. As summarized in Tables 1 and 3, the ore contains 0.45% copper (Cu) and 0.21% copper oxide (CuO).

To further identify the ore's mineralogical composition and determine the association of copper minerals with the gangue, polished section analysis was performed. This method allows a microscopic examination of the ore minerals and accurate identification of mineral phases. The results of Fig. 1 show that the main copper minerals include chalcocite, covellite, and malachite, with minor chalcopyrite. The gangue is primarily silica and pyrite, where silica indicates the dominance of silicate material and pyrite commonly coexists with copper sulfide deposits. The high quartz content in the sample significantly reduces sulfuric acid consumption, which is an important advantage both economically and environmentally.

2.2 Stirred leaching tests and kinetics

Stirred leaching tests were conducted in the Hydrogeology and Environmental Research Laboratory (MEHR) at the University of Tehran, utilizing specialized equipment, including semi-industrial leaching reactors and mechanical stirrers with adjustable speeds. Initially, the samples were subdivided using a riffle splitter and subsequently crushed to obtain five distinct size fractions. Crushing continued until 80% of the material reached the targeted particle size.

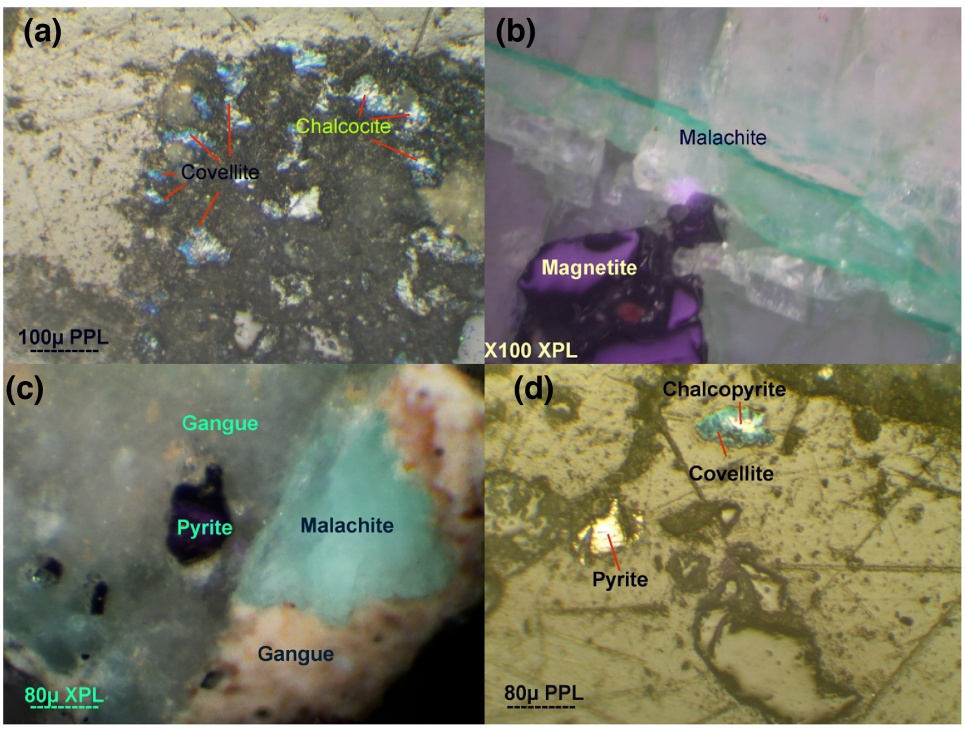

Fig. 1 Polished sections of the Miduk copper mine sample: **a** Malachite and magnetite, **b** Chalcocite and covellite, **c** Chalcopyrite, covellite, and pyrite, **d** Malachite, pyrite, and gangue

A predetermined solids percentage was then mixed with a sulfuric acid solution in a 500 mL volume for each test. Following leaching, solid–liquid separation was performed using a vacuum filter, and the filtrate was analyzed for copper concentration with an atomic absorption spectrophotometer (Shimadzu AA-7000). Copper and iron recoveries were determined using Eq. (1).

$$R\,(\%) = \frac{(C_f \times V)}{(C_i \times m)} \times 100 \tag{1}$$

where R is the recovery (%), C_i is the copper content in the ore sample (%), m is the mass of the ore sample (g), V is the volume of the leaching solution (L), and C_f is the copper concentration in the leaching solution (g L^{-1}). To investigate the dissolution rate and underlying chemical mechanisms, kinetic experiments were performed under varying operating conditions and time intervals. These tests were conducted at specific conditions detailed in Table 4.

2.3 Experimental design

Experimental design, combined with multivariate statistical methods and modeling, is a powerful approach for analyzing and optimizing engineering processes (Cao et al. 2020; Xing et al. 2024). RSM evaluates factor effects and interactions with minimal experiments in leaching studies. The models applied in RSM range from a first-order linear model (Eq. 2) to higher-order polynomial models, such as a second-order model (Eq. 3), which accounts for curvature effects in nonlinear systems.

$$y = \beta_0 + \sum_{i=1}^{n} \beta_i x_i + \varepsilon \tag{2}$$

$$y = \beta_0 + \sum_{i=1}^{n} \beta_i x_i + \sum_{i=1}^{n} \beta_{ii} x_i^2 + \sum_{i \neq j} \beta_{ij} x_i x_j + \varepsilon \tag{3}$$

where n is the number of variables, β_0 is a constant, β_i represents the linear coefficients of the parameters, x_i are the independent variables, β_{ii} denotes the quadratic coefficients, β_{ij} are the interaction coefficients, and ε is the residual associated with the experiments (Harichandan and Mandre 2021; Ayodele et al. 2023).

For the final experimental design using specialized software, five key parameters were selected: acid concentration, particle size distribution, solids content, temperature, and leaching time. These parameters were chosen based on prior studies (Apua and Madiba 2021; Apua et al. 2013; Mohanraj et al. 2022; Harichandan and Mandre 2021). Initial single-factor tests indicated that leaching efficiency was significantly affected by stirring speed, with low recovery at insufficient agitation and diminishing recovery at excessively high speeds. Consequently, 500 rpm was determined as the optimal stirring speed, and all subsequent tests were conducted under this condition. The CCD was employed to evaluate interaction effects among the selected parameters and optimize leaching conditions. Table 5 presents the parameter ranges and their levels in the experimental design.

According to this design, 48 experiments were carried out. The total number of experiments, N, in a CCD is determined using Eq. (4):

$$N = 2^K + 2K + N_c \tag{4}$$

where K is the number of factors and N_c is the number of central points. The experiments were performed in random order.

3 Results and discussion

This study examines the characteristics of copper leaching from a low-grade oxide–sulfide ore in two main phases, with copper recovery selected as the primary performance

Table 5 Factor levels and center values used in stirred leaching experiments (CCD)

Parameter	Unit	Low level	High level	Center level
Acid concentration	mol L^{-1}	1.1	2.3	1.7
Particle size	µm m	100	700	400
Temperature	°C	25	75	50
Solids content	%	10	30	20
Time	min	60	120	90

Table 4 Parameters and levels used in the kinetic experiments

Parameter	Unit	Level 1	Level 2	Level 3	Level 4	Level 5
Acid concentration	mol L^{-1}	0.5	0.8	1.1	1.7	2.3
Agitation speed	rpm	100	200	400	500	600
Particle size	µm	75	100	400	700	1000
Temperature	°C	25	50	60	75	85
Solids content	%	5	10	15	20	30

indicator. Iron recovery was also assessed as part of the experimental framework. In the first phase, the key factors affecting the leaching process were analyzed using Response Surface Methodology (RSM) to determine the optimal operating conditions. The second phase focused on elucidating the leaching mechanism and conducting kinetic modeling to better understand the dissolution process.

3.1 Statistical analysis

The leaching experiments and the experimental matrix designed based on the RSM-CCD model are presented in Table 11. Various models, including Linear, 2FI (two-factor interaction), Quadratic, and Cubic, were applied to the experimental data. Their evaluation using ANOVA at a 95% confidence level $(p\text{-value} < 0.05)$ is summarized in Tables 6 and 7. The results indicate that the Quadratic model, which exhibits a higher coefficient of determination (R^2) and adjusted (R^2) along with a lower p-value, is the most suitable for predicting the rate of copper dissolution. In contrast, the 2FI model provides the best fit for iron recovery.

Based on the experimental data, two second-order polynomial models were developed to predict copper and iron recovery (Eqs. 5 and 6) using coded parameters (see Table 11). These models were specifically employed to evaluate copper and iron recovery under varying leaching process conditions. In this context, in addition to the primary focus on copper recovery, the elevated concentration of dissolved iron was carefully monitored as a secondary parameter to ensure optimized leaching conditions. The high concentration of dissolved iron presents substantial operational challenges in subsequent processing stages, particularly during solvent extraction (SX) and electrowinning (EW). High iron concentrations can reduce extraction efficiency by causing increased reagent consumption and potential emulsion formation. Furthermore, in electrowinning cells, iron ions can negatively affect current efficiency, increase electrical power consumption, and deteriorate cathode quality, significantly reducing overall process productivity. Therefore, iron recovery was carefully monitored and evaluated to minimize iron dissolution and mitigate its related complications in downstream processes.The second-order polynomial model developed in this study, based on laboratory-scale experimental data, serves as a predictive tool to assess the effects of key leaching parameters (acid concentration, temperature, particle size, reaction time, and Solids Content) on copper recovery. Equations 5 and 6 specifically model these individual and interactive effects, providing reliable predictions for copper and iron recovery under laboratory conditions. While the model demonstrates strong predictive capability within the tested range, its application to large-scale industrial processes requires further validation and adjustment using pilot-scale or industrial data. Therefore, it is primarily suited for predicting copper recovery in controlled laboratory conditions, with further studies needed for

Table 6 Statistical analysis of models for copper recovery modeling

Source	Sum of squares	df	Mean square	F-value	p-value
Mean vs Total	2.493E+05	1	2.493E+05	–	–
Block vs Mean	578.48	2	289.24	–	–
Linear vs Block	2622.53	5	524.51	45.17	<0.0001
2FI vs Linear	154.51	10	15.45	1.50	0.1896
Quadratic vs 2FI	179.99	5	36.00	6.92	0.0004 (Suggested)
Cubic vs Quadratic	95.81	15	6.39	1.87	0.1600 (Aliased)
Residual	34.16	10	3.42	–	–
Total	2.530E+05	48	5270.18	–	–
Analysis of Lack of Fit					
Linear	453.76	37	12.26	3.44	0.1684
2FI	299.25	27	11.08	3.11	0.1906
Quadratic	119.26	22	5.42	1.52	0.4136 (Suggested)
Cubic	23.46	7	3.35	0.93	0.5771 (Aliased)
Pure Error	10.71	3	3.57	–	–
Model Summary Statistics					
Source	Std. Dev.	R^2	Adjusted $\mathbf{R}^2$	Predicted $\mathbf{R}^2$	PRESS
Linear	3.41	0.8490	0.8307	0.7920	641.85
2FI	3.21	0.8990	0.8494	0.7900	646.99
Quadratic	2.28	0.9570	0.9242	0.8390	495.90 (Suggested)
Cubic	1.85	0.9880	0.9502	−0.7040	5260.27 (Aliased)

Table 7 Statistical analysis of models for iron recovery modeling

Source	Sum of squares	df	Mean square	F-value	*p*-value
Mean vs Total	330.48	1	330.48	–	–
Block vs Mean	0.4508	2	0.2254	–	–
Linear vs Block	34.44	5	6.89	55.68	<0.0001
2FI vs Linear	2.69	10	0.2695	3.59	0.0032 (Suggested)
Quadratic vs 2FI	3.890	5	0.778	1.04	0.4145
Cubic vs Quadratic	1.59	15	0.1058	3.82	0.0189 (Aliased)
Residual	0.2769	10	0.0277	–	–
Total	370.32	48	7.71	–	–
Analysis of Lack of Fit					
Linear	4.92	37	0.1329	13.48	0.0265
2FI	2.22	27	0.0824	8.35	0.0523 (Suggested)
Quadratic	1.83	22	0.0834	8.46	0.0516
Cubic	0.2473	7	0.0353	3.58	0.1610 (Aliased)
Pure Error	0.0296	3	0.0099	–	–
Model Summary Statistics					
Source	Std. Dev.	R^2	Adjusted $\mathbf{R}^2$	Predicted $\mathbf{R}^2$	PRESS
Linear	0.3517	0.8744	0.8587	0.8117	7.42
2FI	0.2741	0.9428	0.9142	0.8149	6.90 (Suggested)
Quadratic	0.2731	0.9527	0.9148	0.8026	7.77
Cubic	0.1664	0.9930	0.9684	1.0640	35.20 (Aliased)

adapting it to practical industrial applications. These models account for the linear, nonlinear, and interaction effects of key leaching variables, demonstrating high predictive accuracy. Their performance was assessed through analysis of variance (ANOVA), with the results summarized in Tables 8 and 9. The significance of these models lies in their ability to not only improve the copper extraction process but also to reduce costs, time, and chemical reagent consumption, ultimately making the process significantly more economical. Moreover, these models ensure that the process is executed more accurately and efficiently from an environmental perspective. Acid consumption is reduced, waste production is minimized, and higher recovery rates of target metals are achieved, which significantly reduces negative environmental impacts. Therefore, these models serve as an advanced and effective tool that not only optimizes the copper extraction process but also helps in reducing its environmental footprint.

The ANOVA analysis presented in Table 8 confirms that the final model is statistically significant, with an F-value of 28.44 and a *p*-value of less than 0.0001. This suggests a very low probability (0.01 %) that the observed results are due to noise, emphasizing the strong influence of the model's factors on the response and its suitability for data analysis.

The lack of fit (*LackofFit*) value is $F = 1.52$ and $p = 0.4136$, indicating that the model accurately represents the data, and the lack of fit is not statistically significant. These values suggest that noise has minimal impact on the results, confirming the model's robustness.

The mean square (*MS*) for the model is 147.85, which, compared to the mean square error ($MS = 5.20$), underscores the model's high explanatory power. Furthermore, the pure error is relatively small at 10.71, indicating minimal noise and high experimental repeatability.

The most influential parameters, with $p < 0.05$, include E (*E-Solid.C*), B (*B-Time*), C (*C-Gradation*), A (*A-Acid*), and D (*D-Temperature*). Additionally, nonlinear parameters such as A^2 and E^2, along with interaction effects AD, BE, BD, and CE, exhibit the most significant impact on the response. Conversely, parameters with $p > 0.05$, such as AB, AC, and C^2, have minimal influence and can be removed to simplify the model.

Additional statistical results indicate that the coefficient of determination is $R^2 = 0.9579$, meaning the model accounts for approximately 95.79 % of the data variability. The adjusted R^2 is 0.9242, and the predicted R^2 is 0.8394, demonstrating that despite the model's complexity, its predictive performance remains robust. Figure 2d illustrates a comparison between the predicted copper recovery values and the experimental data.

The adequacy precision (*Adeq Precision*), representing the signal-to-noise ratio, is 21.955, significantly exceeding the minimum required value of 4, confirming the model's reliability for exploring the design space. Furthermore, the standard deviation (Std.Dev = 2.28) and the coefficient of variation ($C.V.\% = 3.16$) indicate low data dispersion and high model stability.

Table 8 ANOVA of the second-order response surface model for predicting copper recovery

Source	Sum of squares	df	Mean square	F-value	*p*-value
Block	578.48	2	289.24	–	–
Model	2957.03	20	147.85	28.44	<0.0001 (significant)
A-Acid	84.24	1	84.24	16.20	0.0005
B-Time	486.45	1	486.45	93.57	<0.0001
C-Gradation	480.60	1	480.60	92.45	<0.0001
D-Temperature	23.70	1	23.70	4.56	0.0427
E-Solid.C	1547.54	1	1547.54	297.68	<0.0001
AB	9.89	1	9.89	1.90	0.1800
AC	0.7917	1	0.7917	0.1523	0.6997
AD	23.56	1	23.56	4.53	0.0433
AE	18.27	1	18.27	3.51	0.0726
BC	13.23	1	13.23	2.54	0.1232
BD	26.92	1	26.92	5.18	0.0317
BE	23.88	1	23.88	4.59	0.0420
CD	4.22	1	4.22	0.8116	0.3762
CE	22.09	1	22.09	4.25	0.0498
DE	11.66	1	11.66	2.24	0.1467
A^2	46.41	1	46.41	8.93	0.0062
B^2	16.68	1	16.68	3.21	0.0854
C^2	1.30	1	1.30	0.2495	0.6218
D^2	5.39	1	5.39	1.04	0.3182
E^2	92.12	1	92.12	17.72	0.0003
Residual	129.97	25	5.20	–	–
Lack of Fit	119.26	22	5.42	1.52	0.4136 (Not signif.)
Pure Error	10.71	3	3.57	–	–
Cor Total	3665.48	47	–	–	–
Adeq Precision	21.955				

Figure 2 serves as a diagnostic tool for evaluating model accuracy and adequacy. The figure presents four key analyses: (Fig. 2a) the normal probability plot of residuals, (Fig. 2b) the relationship between standardized residuals and block number, (Fig. 2c) a comparison of experimental (measured) and predicted recovery values, and (Fig. 2d) the distribution of Cook's Distance values. This result shows that no data point has an unusual impact on the model, confirming the high accuracy of the developed model for predicting copper recovery.

Significant parameters influencing iron recovery include A, B, C, and E, as well as their interactions AB, BC, and BE, all of which exhibit a notable impact on the response. These factors and interactions play a crucial role in optimizing iron recovery and must be carefully controlled. Conversely, parameters such as AC, AD, and DE have p-values greater than 0.05 and are not statistically

$$\begin{aligned} R(\mathrm{Cu}) =& 77.81 + 1.51A + 3.65B - 3.62C + 0.80D - 6.51E \\ &+ 0.55AB - 0.15AC + 0.85AD + 0.75AE \\ &- 0.64BC + 0.91BD + 0.86BE + 0.36CD - 0.84CE \\ &- 0.61DE - 2.10A^2 - 1.26B^2 - 0.35C^2 - 0.71D^2 - 2.96E^2 \end{aligned} \quad (5)$$

According to the ANOVA results and model-fitting criteria, the proposed iron recovery model demonstrates high accuracy. The model's F-value of 32.96, with a p-value of less than 0.0001, confirms its strong statistical significance. Furthermore, the model accounts for a sum of squares of 37.13, explaining a substantial portion of data variation, while the residual error remains low at 2.25, indicating that the model effectively minimizes unexplained variance. With $R^2 = 0.9428$ and an adjusted $R^2 = 0.9142$, the model maintains strong explanatory power despite its complexity. Additionally, the predicted R^2 value of 0.8149 suggests that the model accurately predicts approximately 81.49% of the data variability.

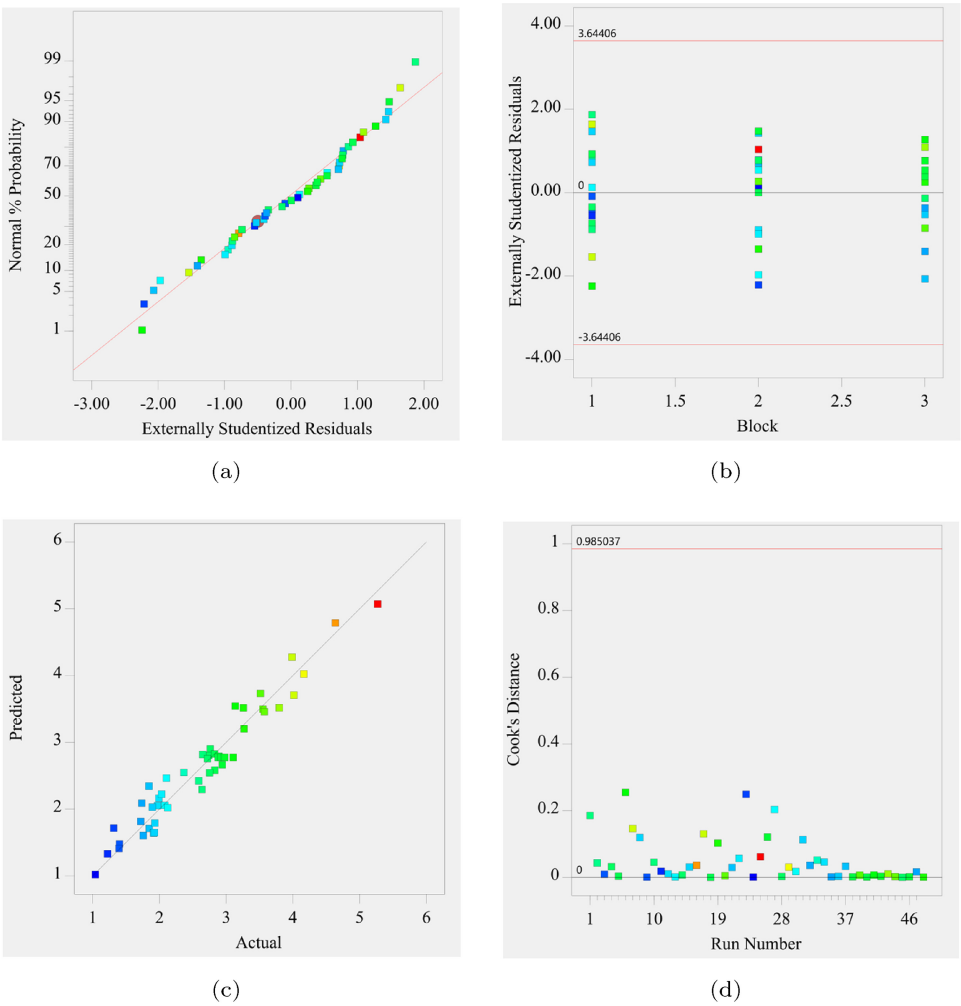

Fig. 2 Validation of the second-order model proposed for predicting copper recovery

significant, suggesting that they can be removed to simplify the model without compromising predictive accuracy.

The same diagnostic plots used for copper recovery were employed to evaluate the model's performance in predicting iron recovery. As illustrated in Fig. 3, the model provides reliable predictions, with no abnormal or excessively influential data points, confirming its robustness and predictive capability.

costs. The solids percentage must be controlled: high solids increase viscosity, limiting mass transfer, while low solids reduce reactant concentrations, lowering efficiency. Optimal conditions balance leaching time and solids content for effective dissolution and cost efficiency (Mohanraj et al. 2022; Harichandan and Mandre 2021).

Temperature has a strong influence on copper recovery, as higher temperatures accelerate reaction rates and

$$\begin{aligned} R(\mathrm{Fe}) = {} & 2.63 + 0.49A + 0.69B - 0.45C + 0.01D - 0.28E \\ & + 0.18AB - 0.03AC + 0.07AD + 0.01AE - 0.17BC \\ & + 0.02BD - 0.10BE - 0.04CD - 0.002CE - 0.02DE \end{aligned} \tag{6}$$

3.2 Operational parameters

Figures 4 and 5 illustrate the effects of various parameter interactions on copper recovery. In Fig. 4a, Longer leaching time improves copper recovery, but excessive time increases

improve dissolution efficiency (Fig. 4b). Excessively high temperatures may dissolve undesirable compounds or form problematic precipitates, reducing product quality. Lower temperatures slow down reaction kinetics, reducing recovery. Acid concentration is crucial for providing ions for dissolution, but excessive acid can dissolve impurities like iron,

Table 9 ANOVA of the Quadratic Response-Surface Model for Predicting Iron Recovery

Source	Sum of squares	df	Mean square	F-value (*p*-value)
Block	0.4508	2	0.2254	–
Model	37.13	15	2.48	32.96 (<0.0001)*
A-Acid	8.98	1	–	119.51 (<0.0001)*
B-Time	14.88	1	–	198.03 (<0.0001)*
C-Gradation	7.59	1	–	101.11 (<0.0001)*
D-Temperature	0.0054	1	–	0.0723 (0.7899)
E-Solid.C	2.99	1	–	39.75 (<0.0001)*
AB	1.04	1	–	13.82 (0.0008)*
AC	0.0298	1	–	0.3965 (0.5337)
AD	0.1981	1	–	2.64 (0.1149)
AE	0.0001	1	–	0.0015 (0.9695)
BC	0.9775	1	–	13.01 (0.0011)*
BD	0.0000	1	–	0.0004 (0.9840)
BE	0.3720	1	–	4.95 (0.0337)*
CD	0.0565	1	–	0.7516 (0.3928)
CE	0.0002	1	–	0.0026 (0.9595)
DE	0.0225	1	–	0.2991 (0.5885)
Residual	2.25	30	0.0751	–
Lack of Fit	2.22	27	0.0824	8.35 (0.0523)
Pure Error	0.0296	3	0.0099	–
Cor Total	39.84	47	–	–
Adeq Precision	19.12	–	–	–

*Significant at $p < 0.05$

complicating downstream processes and lowering product purity (Ajiboye et al. 2019; Shi et al. 2020).

Figure 5a Finer particles increase recovery by providing more surface area, but excessive grinding raises costs. A moderate particle size is usually the most cost-effective. Lower solids fractions improve solution access, but too low a fraction reduces efficiency (Antonijević et al. 2004).

Figure 5b illustrates the effect of temperature and leaching time on copper recovery. Higher temperatures improve recovery but excess heat can cause impurities. Leaching time must be balanced-too short leads to incomplete dissolution, while too long increases costs. Optimal conditions require careful balance of temperature, time, particle size, and solids fractions (Antonijević et al. 2004).

Figure 6 illustrates the sensitivity of copper recovery *R*(Cu) to different process variables. The curvature of each line represents the strength of the variable's influence on the response. Variables *B* (leaching time) and *E* (solids fraction) exhibit the highest curvature, indicating that fluctuations in these parameters have a substantial impact on copper recovery. Variable *C* (particle size) also plays a significant role, though its effect is somewhat less pronounced compared to *B* and *E*. In contrast, variables *A* (acid concentration) and *D* (temperature) display more linear and gradual slopes, suggesting a relatively weaker influence on the response. This analysis helps prioritize key parameters-*B*, *E*, and *C*-for precise control to optimize copper recovery.

Figure 7 illustrates the influence of different variables on iron recovery *R*(Fe). Although iron dissolution is minimal in the process, maintaining appropriate conditions to limit its extraction remains essential for process efficiency and product purity. Solids fraction and leaching time exhibit similar trends (Fig. 7a). A lower solids fraction decreases the likelihood of iron dissolution; however, an excessively low solids fraction may also disrupt the primary copper leaching reactions. Optimal conditions are achieved when these parameters are carefully balanced to minimize iron dissolution while ensuring efficient copper recovery.

Figure 7b Acid concentration and leaching time must be optimized to maximize copper dissolution without causing excessive iron extraction. Figure 7c evaluates the interaction between particle size distribution and time. Moderate particle sizes reduce grinding costs, and excessive leaching time may increase iron dissolution. Precise control of both is essential for an efficient process (Ajiboye et al. 2019; Mohanraj et al. 2022; Antonijević et al. 2004).

3.3 Optimized recovery conditions

The optimal conditions for maximizing copper extraction while minimizing iron dissolution were determined through

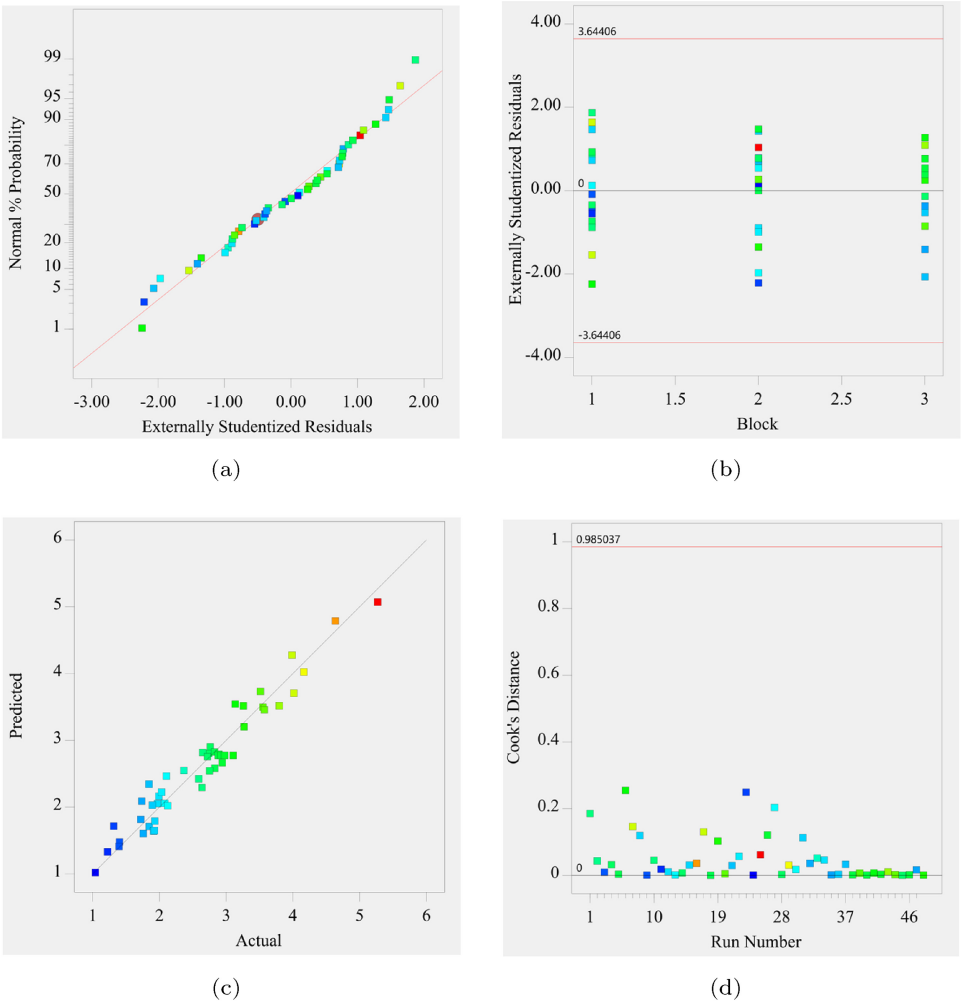

Fig. 3 Validation of the second-order model proposed for predicting iron recovery

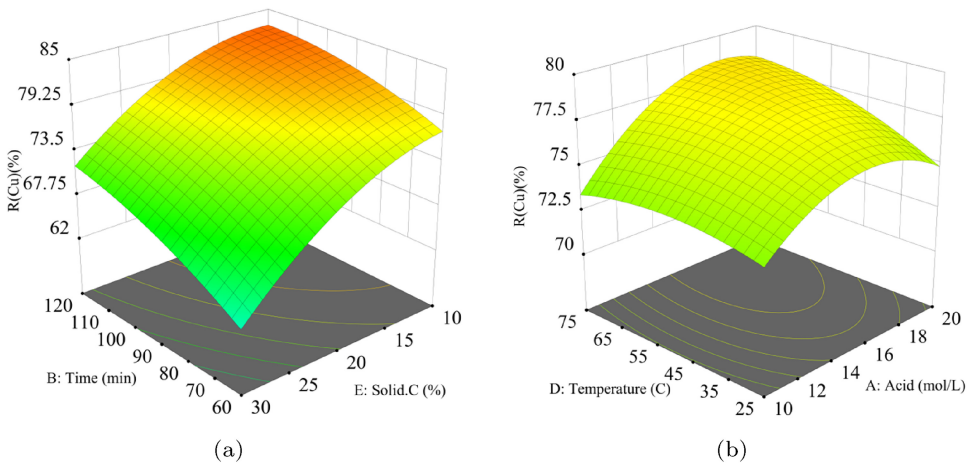

Fig. 4 **a** Time–solids fraction interaction; **b** Acid concentration–temperature interaction for copper recovery

the analysis of process parameters. Under these optimized conditions, copper recovery $(R(\mathrm{Cu}))$ reaches 80 %, while iron recovery $(R(\mathrm{Fe}))$ is minimized to 3 %. The key operating parameters include an acid concentration of 1.21 mol L^{-1}, a leaching time of 108 min, a particle size of 438 µm, a temperature of 45 °C, and a solids content of 18.2 %. The high desirability value of 0.982 indicates a strong alignment with process objectives, ensuring an optimal balance between efficient copper recovery and minimal iron dissolution. This optimization enhances process sustainability and

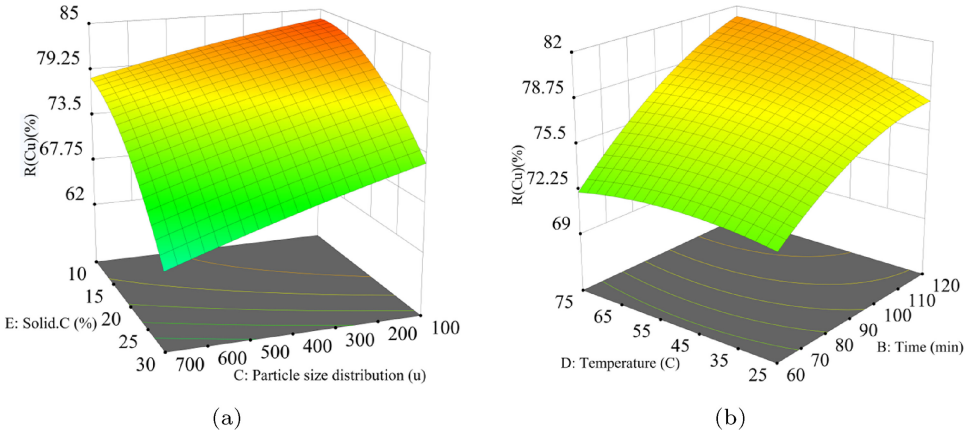

Fig. 5 **a** Particle size–solids fraction interaction; **b** Time–temperature interaction for copper recovery

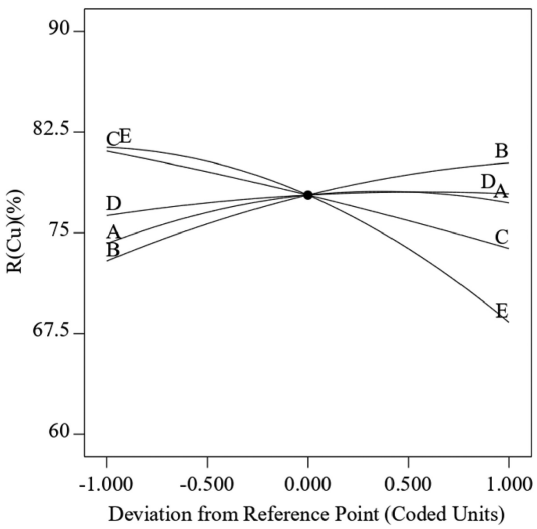

Fig. 6 Perturbation plot showing the influence of different variables on copper recovery

operational efficiency. Sustainability, in this context, refers to the long-term environmental and economic benefits of the process. By carefully controlling factors like particle size, leaching time, and acid concentration, the process minimizes waste production, reduces energy consumption, and lowers the need for excessive reagent use, which in turn lessens environmental impacts such as pollution and resource depletion. Moreover, achieving optimal conditions leads to cost savings, as it minimizes the unnecessary use of resources, making the process more economically viable over time. The results of this study can be applied to optimize copper extraction processes in real-world settings, providing more efficient methods for processing low-grade ores while reducing costs. By precisely adjusting parameters such as acid concentration, temperature, and reaction time, industries can achieve higher recovery rates and better resource utilization, which ultimately leads to more sustainable mining operations.

Environmental concerns play a significant role in the application of these findings. For example, optimized leaching conditions can reduce the environmental footprint of copper processing. Reducing acid consumption, lowering energy usage, and minimizing waste generation are aspects that can be achieved by applying these findings. Furthermore, optimizing copper recovery in this way can help mitigate the negative environmental impacts typically associated with conventional extraction methods, such as excessive water and chemical use, land degradation, and pollution.

To fully assess the impact of these results, future research is required to validate the findings under real industrial conditions. While the laboratory data demonstrate the model's predictive capability, its practical application at larger scales would require further adjustments based on pilot-scale or industrial data. Additionally, conducting field trials and measuring environmental impacts on a broader scale will help improve the method and ensure that these approaches are both economically viable and environmentally sustainable.

3.4 Leaching kinetics and mechanisms

The kinetics of the leaching process were analyzed using the Shrinking Core Model (SCM), which assumes that reactions initiate at the particle surface and progress inward as the unreacted core gradually diminishes. Figure 13 provides a schematic representation of this model (Astuti et al. 2016; Boukerche et al. 2010; Tan et al. 2017; Faraji et al. 2022). The SCM identifies three main mechanisms governing the reaction rate: liquid-film diffusion, where the reagent diffuses through a thin liquid layer around the particle; product-layer diffusion, where a dense product layer restricts mass transfer; and surface chemical reaction, where the rate-limiting step occurs at the unreacted core, where the chemical reaction happens.

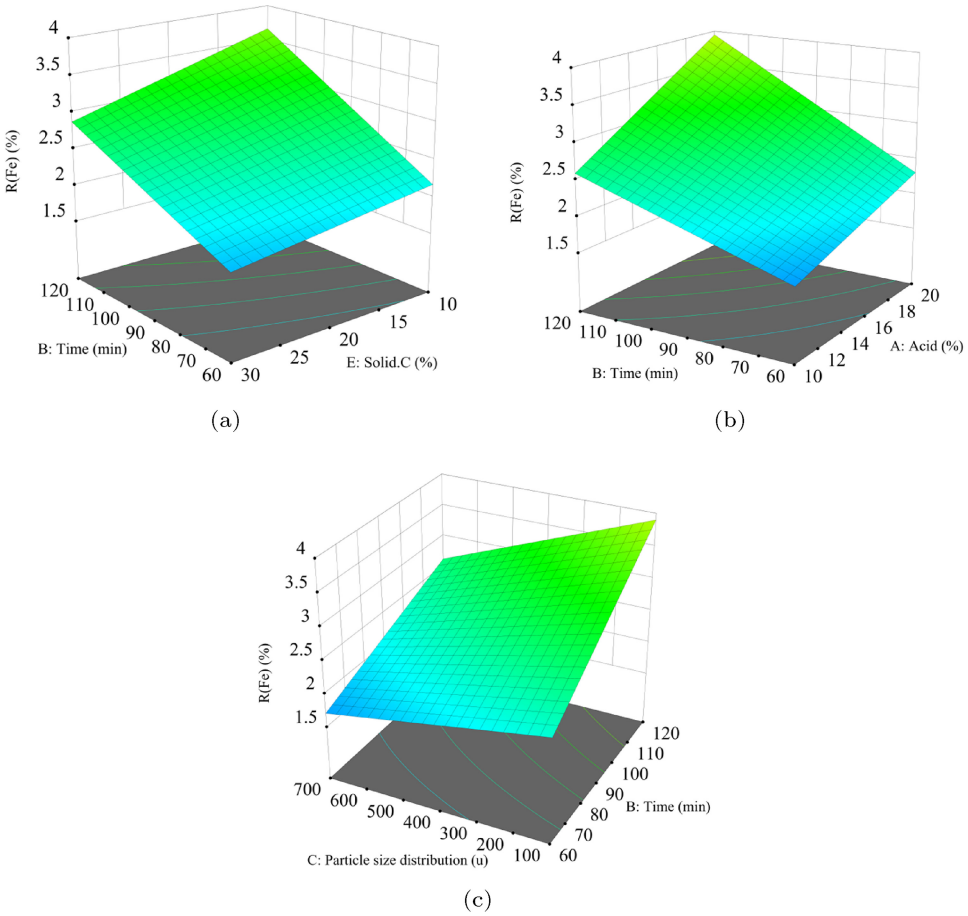

Fig. 7 **a** Effect of solids fraction–time, **b** Acid concentration–time, and **c** Particle size distribution–time on iron recovery

These mechanisms are mathematically described in Eqs. (7), (8), and (9). Additionally, Eq. (10) presents an extended kinetic model for fluid–solid reactions, incorporating resistance within both the product layer and the interface between the unreacted core and the reaction layer (Wadsworth and Sohn 1979; Dickinson and Heal 1999). This refined approach offers a more accurate representation of leaching kinetics, facilitating process optimization, particularly in systems where diffusion and interface resistance significantly influence the overall reaction rate.

$$1-(1-x)^{1/3}=k_{\text{film}}\,t, \tag{7}$$

$$1-3(1-x)^{2/3}+2(1-x)=k_{\text{prod}}\,t, \tag{8}$$

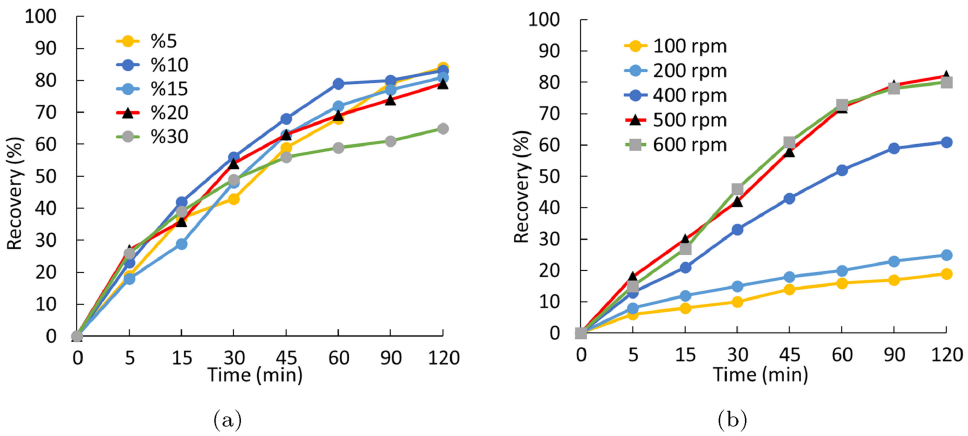

Fig. 8 **a** Effect of solids percentage; **b** effect of stirring rate on the leaching process

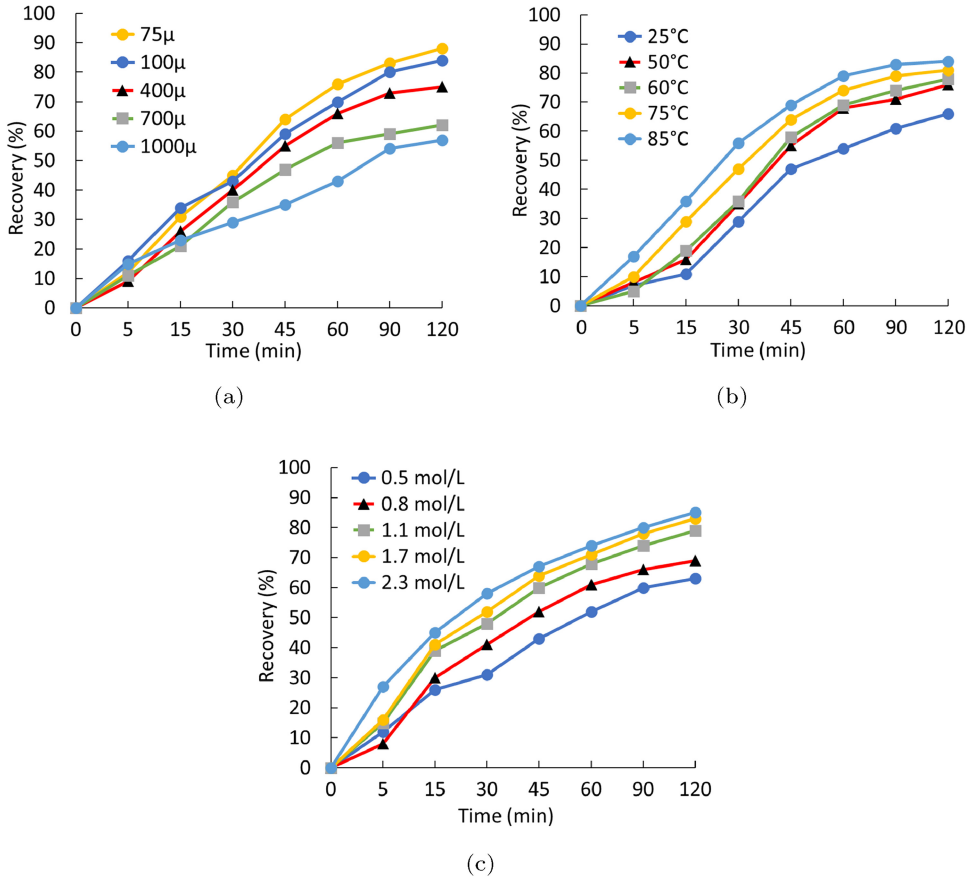

Fig. 9 **a** Effect of particle size, **b** effect of temperature, and **c** effect of acid concentration on the leaching process

$$1-(1-x)^{1/3}=k_{\text{chem}}\,t, \tag{9}$$

$$\frac{1}{5}\times(1-x)^{-5/3}-\frac{1}{4}\times(1-x)^{-4/3}+\frac{1}{20}=k_{\text{Dickinson}}\,t, \tag{10}$$

where x is the fraction of copper extracted, t is the leaching time in minutes, and the rate constants k_{film}, k_{prod}, k_{chem}, and $k_{\text{Dickinson}}$ correspond to surface chemical reaction, liquid-film diffusion, product-layer diffusion, and the Dickinson equation, respectively. The leaching kinetic tests were fitted and analyzed using Eqs. (7)–(10) (Dickinson and Heal 1999; Aghazadeh and Nabizadeh 2015). The overall reaction rate is determined by the slowest step, which serves as the rate-limiting factor.

Figures 8 and 9 present the results of copper leaching tests conducted using the One Factor at a Time (OFAT) method to evaluate the effects of solids percentage, stirring rate, temperature, particle size distribution, and acid concentration on the leaching process. In each test, only one factor was varied while maintaining constant conditions for the others, specifically an acid concentration of 1.1 mol L^{-1}, a particle size of 400 µm, a temperature of 50 °C, a stirring rate of 500 rpm, and a solids content of 20 %. The slopes of the lines representing the reaction-rate equations (apparent rate constants) illustrate how each parameter influences the rate law and clarify the role of each factor in governing the overall leaching mechanism.

The shrinking-core model, incorporating four primary mechanisms-surface chemical reaction (Eq. 7), liquid-film diffusion (Eq. 8), product-layer diffusion (Eq. 9), and the Dickinson model (Eq. 10)-was applied to analyze the leaching kinetics. These models were fitted to the experimental leaching data, and kinetic parameters, including apparent rate constants and correlation coefficients, were determined for each mechanism.

To assess the governing mechanisms, the left-hand side of Eqs. (7), (8), (9), and (10) was plotted against reaction time for each operating factor, namely temperature, acid concentration, solids content, stirring rate, and particle size. Figure 10 illustrates the effect of temperature on all four principal mechanisms of the shrinking-core model, where the slope of each linear plot represents the reaction-rate constants at different temperatures, while the correlation of the data is also displayed. In addition to temperature, the influence of other operational parameters on apparent rate constants and correlation coefficients was analyzed. These results are presented numerically in Table 10, facilitating a detailed comparison of how each factor influences the process and identifying the dominant leaching mechanism.

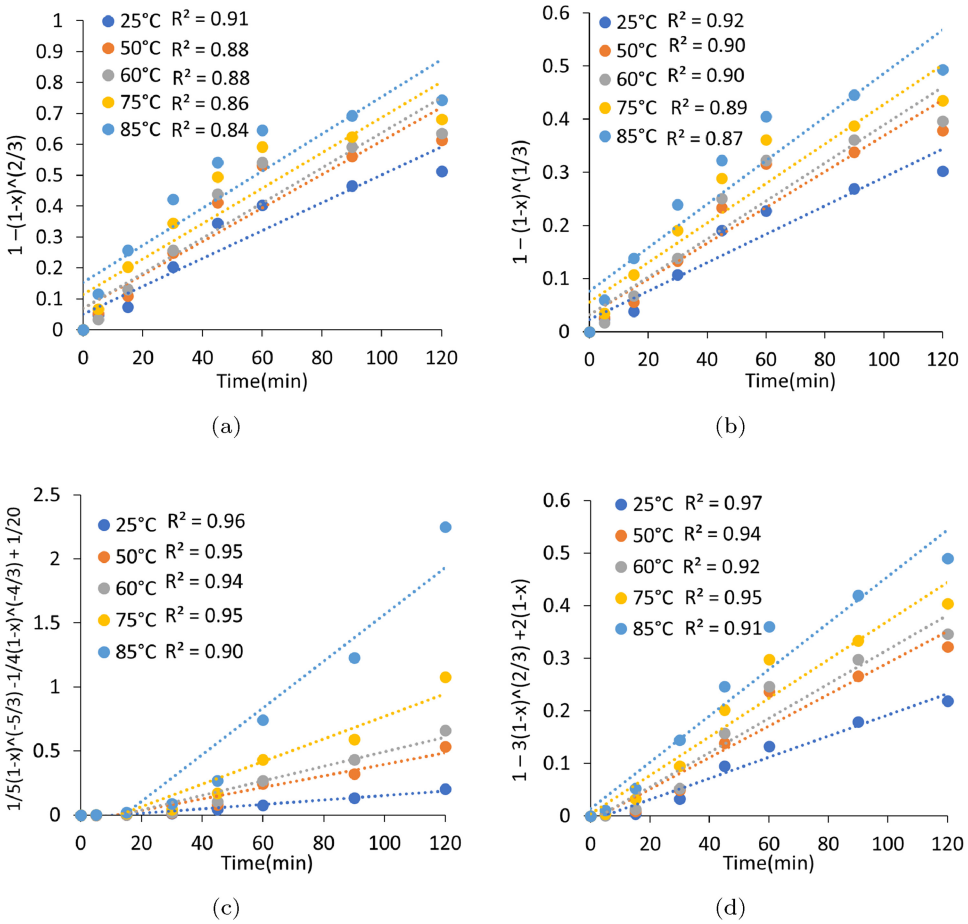

Fig. 10 Effect of temperature on the four main mechanisms in the shrinking-core model: **a** fluid-film diffusion , **b** surface chemical reaction, **c** Dickinson model , and **d** product-layer diffusion

3.5 Activation energy and kinetic model refinement

The R^2 values presented in Table 10 indicate that both the Dickinson model and the product-layer diffusion model exhibit a strong correlation with the experimental data, yielding higher R^2 values compared to the surface chemical reaction and liquid-film diffusion models. However, due to the close similarity in R^2 values, determining the dominant mechanism solely based on these results remains inconclusive, necessitating an alternative approach for precise identification.

To further refine the analysis, an Arrhenius-based activation energy study was conducted to gain deeper insights into the leaching process mechanism and kinetics. Activation energy (E_a) varies significantly between diffusion-controlled and chemically controlled reactions, providing valuable indications of the rate-limiting step. Although activation energy alone cannot definitively determine the controlling mechanism, it serves as a crucial diagnostic tool in kinetic analysis (Habashi 1980; Ajiboye et al. 2019; Apua and Madiba 2021; Babu et al. 2002; Künkül 1994). According to Fig. 11, the calculated activation energy for the Dickinson model is 32.627 kJ mol^{-1}; for the product-layer diffusion model, it is 11.134 kJ mol^{-1}; for fluid-film diffusion, 4.197 kJ mol^{-1}; and for surface chemical reaction, 5.800 kJ mol^{-1}. These values suggest that the Dickinson model requires a significantly higher activation energy to initiate the process, indicating that this mechanism likely governs the leaching kinetics.

By integrating Eq. (10) and The Arrhenius equation and the activation energy derived from it and incorporating the influence of reaction parameters on the rate constant, the final kinetic model is expressed as Eq. (11). In this formulation, *SS*, *SC*, PSD, and *C* correspond to the stirring speed, solids content, particle size distribution, and acid concentration, respectively. The coefficients *a*, *b*, *c*, and *d* represent the reaction orders for each parameter and were determined from the data in Table 10 by plotting ln *k* against ln(parameter). The estimated values for these coefficients are 1.86, −1.24, −1.19, and 1.57, respectively. Equation (12) presents the final form of the kinetic model, incorporating the experimentally determined parameters and their respective exponents.

$$k_{\text{Dickinson}}\, t \;=\; A_0 \exp\!\left(-\frac{E_a}{RT}\right) (SS)^{a} \; (SC)^{b} \; (\text{PSD})^{c} \; (C)^{d}\, t \tag{11}$$

Table 10 Apparent reaction-rate constants and correlation coefficients for the four shrinking-core mechanisms

Param.[1]	FD		PLD		Dickinson		SCR	
	k	R^2	*k*	R^2	*k*	R^2	*k*	R^2
Sol.C (%)								
5	0.0056	0.92	0.0038	0.91	0.0125	0.89	0.0020	0.74
10	0.0053	0.79	0.0037	0.94	0.0118	0.94	0.0031	0.87
15	0.0054	0.86	0.0035	0.93	0.0097	0.95	0.0035	0.90
20	0.0048	0.81	0.0031	0.96	0.0028	0.97	0.0036	0.84
30	0.0034	0.70	0.0017	0.88	0.0015	0.93	0.0038	0.95
Temp. (°C)								
25	0.0045	0.91	0.0020	0.97	0.0017	0.96	0.0027	0.92
50	0.0054	0.88	0.0033	0.94	0.0045	0.95	0.0034	0.90
60	0.0057	0.88	0.0036	0.92	0.0057	0.95	0.0036	0.90
75	0.0057	0.86	0.0037	0.95	0.0088	0.94	0.0037	0.87
85	0.0060	0.84	0.0044	0.91	0.0182	0.90	0.0041	0.89
Acid (mol/L)								
0.5	0.0038	0.89	0.0017	0.96	0.0013	0.96	0.0023	0.92
0.8	0.0045	0.84	0.0022	0.93	0.0024	0.98	0.0027	0.87
1.1	0.0050	0.85	0.0031	0.95	0.0058	0.92	0.0032	0.89
1.7	0.0054	0.84	0.0036	0.92	0.0114	0.91	0.0036	0.90
2.3	0.0052	0.81	0.0038	0.93	0.0121	0.90	0.0035	0.88
Stir. Rate (rpm)								
100	0.0010	0.84	0.0001	0.94	0.0003	0.97	0.0005	0.85
200	0.0012	0.83	0.0002	0.95	0.0005	0.99	0.0007	0.84
400	0.0038	0.89	0.0016	0.96	0.0014	0.96	0.0022	0.91
500	0.0050	0.88	0.0031	0.92	0.0049	0.93	0.0032	0.92
600	0.0056	0.85	0.0036	0.97	0.0097	0.94	0.0036	0.90
Part. Size (μm)								
75	0.0063	0.90	0.0046	0.95	0.0201	0.86	0.0016	0.88
100	0.0057	0.91	0.0038	0.91	0.0109	0.87	0.0023	0.87
400	0.0050	0.87	0.0027	0.92	0.0039	0.94	0.0031	0.91
700	0.0039	0.85	0.0014	0.94	0.0013	0.97	0.0037	0.94
1000	0.0028	0.86	0.0010	0.93	0.0007	0.91	0.0043	0.95

Abbreviations: *Sol.C* Solid Content, *Temp.* Temperature, *Stir. Rate* Stirring Rate, *Part. Size* Particle Size, *PLD* Product-Layer Diffusion, *SCR* Surface Chemical Reaction

$$k_{\text{Dickinson}}\, t \;=\; A_0 \exp\!\left(-\frac{32.627\times 10^3}{8.314\,T}\right)\left(SS\right)^{1.86}\left(SC\right)^{-1.24}\left(\text{PSD}\right)^{-1.19}\left(C\right)^{1.57} t \tag{12}$$

Figure 12 presents a scatter plot comparing the experimental data with the predictions of the developed kinetic model. The high correlation coefficient $\mathrm{R}^2 = 0.92$ confirms a strong agreement between the experimental results and the model's predictions, demonstrating its reliability and robustness in simulating the copper dissolution process. The model accurately captures leaching dynamics, factoring in

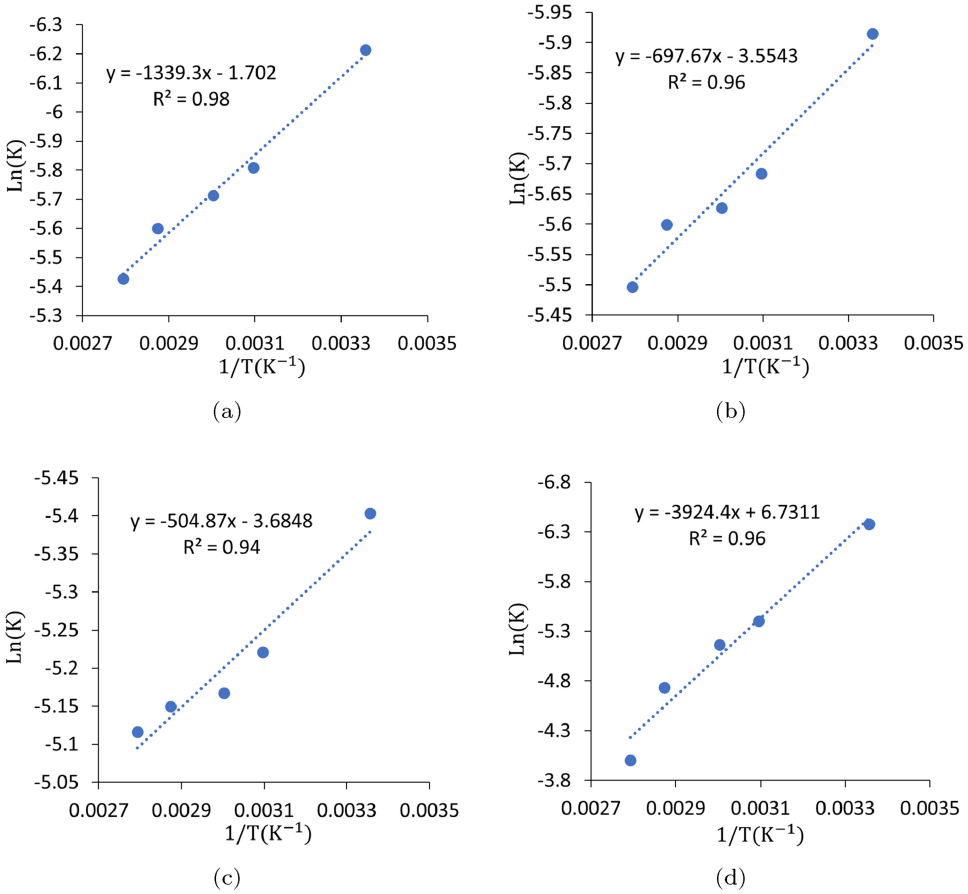

Fig. 11 Arrhenius plots: **a** product-layer diffusion, **b** surface chemical reaction, **c** fluid-film diffusion, and **d** Dickinson model

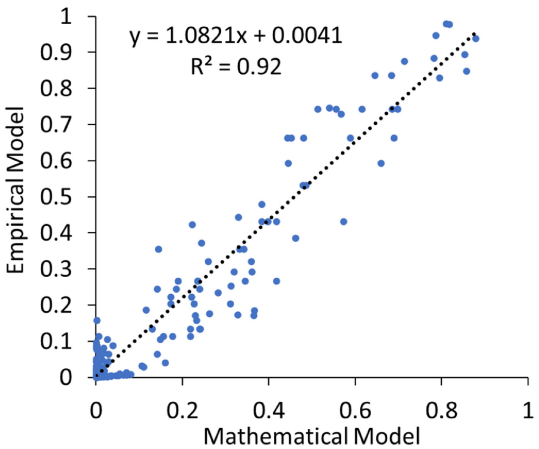

Fig. 12 Comparison between the experimental kinetic model and the developed mathematical model

key parameters like stirring speed, solids content, particle size, and acid concentration. It serves as a valuable tool for optimizing conditions and improving process efficiency.

4 Conclusions

This study determined the optimal conditions for the copper leaching process, which include an acid concentration of 1.21 mol L^{-1}, a leaching time of 108 min, a particle size of 438 µm, a temperature of 45 °C, and a solids content of 18.2 %. Under these conditions, copper recovery R(Cu) reaches 80 %, while iron dissolution R(Fe) remains below 3 %, ensuring an efficient separation and extraction process.

The kinetic study evaluated four main shrinking-core mechanisms: fluid-film diffusion, product-layer diffusion, surface chemical reaction, and the Dickinson model. Among these, the Dickinson model and product-layer diffusion exhibited the highest correlation coefficients R^2, indicating their strong alignment with the experimental data.

Further analysis using activation energy confirmed that the Dickinson model, with an activation energy of 32.627 kJ mol^{-1}, predominantly governs the leaching process. The other mechanisms demonstrated lower activation energy values, reinforcing the conclusion that the process is primarily controlled by the Dickinson model.

Finally, a kinetic model was developed, incorporating key operational parameters such as stirring speed, solids content, particle size, acid concentration, and activation energy. With a high correlation coefficient of $R^2 = 0.92$, the model accurately predicts the leaching process and effectively simulates real-world system behavior, providing a reliable framework for process optimization.

Funding Open Access funding enabled and organized by Projekt DEAL.

Data availability The datasets generated and/or analyzed during the current study are available within the manuscript.

Declarations

Conflict of interest The authors declare no Conflict of interest.

Consent for publication All authors have provided their consent for publication of this work.

Appendix

See Fig. 13 and Table 11.

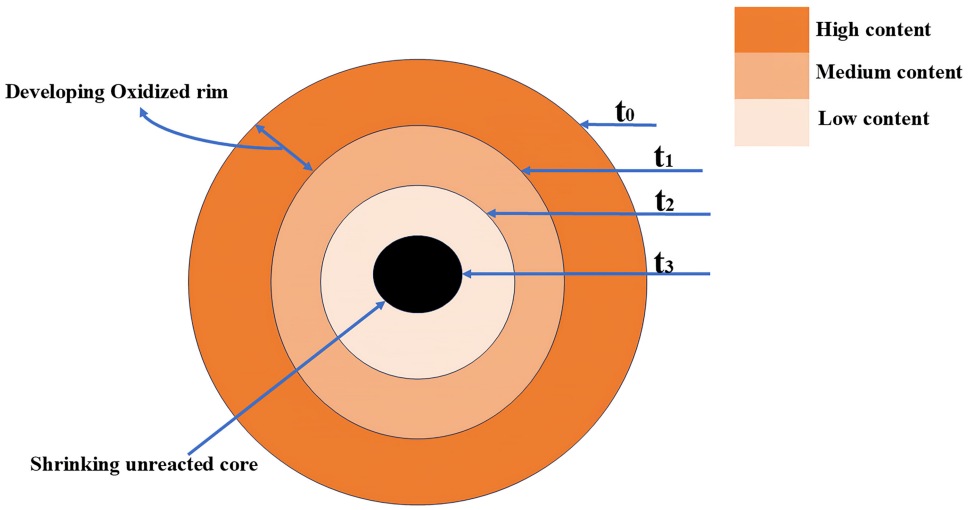

Fig. 13 Schematic of leaching particles using a shrinking-core model where the particle size remains constant throughout the reaction

Table 11 RSM-CCD matrix and copper/iron recoveries

Block	Run	Acid (mol L^{-1})	Time (min)	PSD (μm)	T (°C)	Solid (%)	R(Cu) (%)	R(Fe) (%)
Block 1	1	2.3	60	100	25	30	63.33	2.63
Block 1	2	1.1	120	700	25	10	73.82	2.58
Block 1	3	1.1	60	700	75	10	72.48	1.46
Block 1	4	2.3	60	100	75	10	75.01	2.72
Block 1	5	1.7	90	400	50	20	78.72	2.95
Block 1	6	1.1	120	100	75	10	81.83	3.13
Block 1	7	2.3	120	700	75	10	77.71	4.01
Block 1	8	1.1	60	100	75	30	56.62	1.92
Block 1	9	1.1	120	700	75	30	57.27	1.39
Block 1	10	2.3	120	700	25	30	61.38	2.64
Block 1	11	1.7	90	400	50	35	62.24	1.81
Block 1	12	2.3	60	700	25	10	66.63	1.97
Block 1	13	1.1	60	100	25	10	71.92	2.07
Block 1	14	1.7	90	850	50	20	75.94	1.73
Block 1	15	2.3	60	700	75	30	57.21	1.91
Block 1	16	2.3	120	100	25	10	81.06	4.67
Block 1	17	2.3	120	100	75	30	75.64	3.98
Block 2	18	1.7	135	400	50	20	83.84	3.51
Block 2	19	2.3	120	700	25	10	73.61	3.25
Block 2	20	1.1	120	100	25	10	78.24	3.54
Block 2	21	2.3	60	700	25	30	56.23	1.79
Block 2	22	1.1	120	700	75	10	74.26	2.03
Block 2	23	1.7	90	400	50	20	76.32	3.11
Block 2	24	1.1	60	700	75	30	51.29	1.04
Block 2	25	1.1	60	100	25	30	64.66	1.29
Block 2	26	1.7	90	400	50	20	78.08	2.91
Block 2	27	2.3	60	100	75	30	64.02	2.12
Block 3	35	1.7	45	400	50	20	72.09	1.71
Block 3	36	0.8	90	400	50	20	71.08	1.89
Block 3	37	1.1	60	700	25	30	55.14	1.22
Block 3	38	1.7	90	400	87.5	20	81.25	2.88
Block 3	39	2.3	120	700	75	30	70.48	2.82
Block 3	40	1.7	90	400	50	20	79.04	2.69
Block 3	41	2.3	120	100	75	10	86.42	5.26
Block 3	42	1.7	90	400	50	20	80.83	2.97
Block 3	43	1.1	120	700	25	30	58.46	1.96
Block 3	44	1.7	90	50	50	20	83.91	3.57
Block 3	45	1.7	90	400	12.5	20	75.72	2.71
Block 3	46	1.1	120	100	75	30	71.86	2.94
Block 3	47	2.3	120	100	25	30	72.74	4.17
Block 3	48	1.7	90	400	50	5	84.93	3.26

References

Aghazadeh V, Nabizadeh A (2015) Study and suitable method selection for copper leaching from its oxide ore: Case study of ghare tappeh copper ore. J Mining Engin 10(28):35–42.

Ajiboye EA, Panda PK, Adebayo AO, Ajayi OO, Tripathy BC, Ghosh MK, Basu S (2019) Leaching kinetics of Cu, Ni and Zn from waste silica rich integrated circuits using mild nitric acid. Hydrometallurgy 188:161–168. https://doi.org/10.1016/j.hydromet.2019.06.016

Antonijević MM, Dimitrijević MD, Stevanović ZO, Serbula SM, Bogdanovic GD (2008) Investigation of the possibility of copper recovery from the flotation tailings by acid leaching. J Hazard Mater 158(1):23–34. https://doi.org/10.1016/j.jhazmat.2008.01.063

Antonijević MM, Janković ZD, Dimitrijević MD (2004) Kinetics of chalcopyrite dissolution by hydrogen peroxide in sulphuric acid. Hydrometallurgy 71(3–4):329–334. https://doi.org/10.1016/S0304-386X(03)00082-3

Apua MC, Kime MB, Mubiayi MP (2013) A study of leaching of copper oxide ore by sulphuric acid. In: Proceedings of the 52nd Conference of Metallurgists, Montreal, Quebec, Canada. pp. 83-91

Apua MC, Madiba MS (2021) Leaching kinetics and predictive models for elements extraction from copper oxide ore in sulphuric acid. J Taiwan Inst Chem Eng 121:313–320. https://doi.org/10.1016/j.jtice.2021.04.005

Astuti W, Hirajima T, Sasaki K, Okibe N (2016) Comparison of atmospheric citric acid leaching kinetics of nickel from different Indonesian saprolitic ores. Hydrometallurgy 161:138–151. https://doi.org/10.1016/j.hydromet.2015.12.015

Ayodele TJ, Daniyan AA, Adeleke AA, Ola-Omole OO (2023) Optimization of leaching parameters for the extraction of copper from hematite-dominated copper ore using Response Surface Methodology (RSM). Nig J Tech 42(3):353–363. https://doi.org/10.4314/njt.v42i3.8

Babu MN, Sahu KK, Pandey BD (2002) Zinc recovery from sphalerite concentrate by direct oxidative leaching with ammonium, sodium and potassium persulphates. Hydrometallurgy 64(2):119–129. https://doi.org/10.1016/S0304-386X(02)00030-0

Bai S, Fu X, Li C, Wen S (2018) Process improvement and kinetic study on copper leaching from low-grade cuprite ores. Physicochem Prob Mineral-Proc 54(2):300–310.

Bayati B, Azizi A, Karamoozian M (2018) A comprehensive study of the leaching behavior and dissolution kinetics of copper oxide ore in sulfuric acid lixiviant. Sci Iran 25:1412–1422

Bingöl D, Canbazoğlu M (2004) Dissolution kinetics of malachite in sulphuric acid. Hydrometallurgy 72(1–2):159–165. https://doi.org/10.1016/j.hydromet.2003.10.002

Boukerche I, Habbache N, Alane N, Djerad S, Tifouti L (2010) Dissolution of cobalt from CoO/Al2O3 catalyst with mineral acids. Ind Eng Chem Res 49(14):6514–6520. https://doi.org/10.1021/ie901444y

Cao V, Schaffer M, Taherdangkoo R, Licha T (2020) Solute reactive tracers for hydrogeological applications: A short review and future prospects. Water 12(3):653. https://doi.org/10.3390/w12030653

Chen T, Lei C, Yan B, Xiao XM (2014) Metal recovery from the copper sulfide tailing with leaching and fractional precipitation technology. Hydrometallurgy 147:178–182. https://doi.org/10.1016/j.hydromet.2014.05.018

Crundwell FK (2014) The mechanism of dissolution of minerals in acidic and alkaline solutions: Part III. Application to oxide, hydroxide and sulfide minerals. Hydrometallurgy 149:71–81. https://doi.org/10.1016/j.hydromet.2014.06.008

Davenport WG, King M, Schlesinger M, Biswas AK (2002) Chemical metallurgy of copper recycling. Extractive Metallurgy of Copper. Elsevier, pp 355–365. https://doi.org/10.1016/b978-008044029-3/50024-1

Dickinson CF, Heal GR (1999) Solid–liquid diffusion controlled rate equations. Thermochim Acta 340:89–103. https://doi.org/10.1016/S0040-6031(99)00256-7

Faraji F, Alizadeh A, Rashchi F, Mostoufi N (2022) Kinetics of leaching: A review. Rev Chem Eng 38(2):113–148. https://doi.org/10.1515/revce-2019-0073

Free M (2013) Hydrometallurgy: Fundamentals and applications. John Wiley & Sons, Hoboken, NJ, USA.

Gupta CK, Mukherjee TK (2017) Hydrometallurgy in Extraction Processes, Volume II. CRC Press, Boca Raton, FL.

Habashi F (1980) Principles of extractive metallurgy (2nd edn). Gordon and Breach Science Publ., New York

Haghighi HK, Moradkhani D, Sedaghat B, Rajaie Najafabadi M, Behnam-fard A (2013) Production of copper cathode from oxidized copper ores by acidic leaching and two-step precipitation followed by electrowinning. Hydrometallurgy 133:111–117. https://doi.org/10.1016/j.hydromet.2012.12.004

Han BS, Altansukh B, Haga K, Stevanović Z, Jonović R, Avramović L, Urosević D, Takasaki Y, Masuda N, Ishiyama D, Shibayama A (2018) Development of copper recovery process from flotation tailings by a combined method of high–pressure leaching–solvent extraction. J Hazard Mater 352:192–203. https://doi.org/10.1016/j.jhazmat.2018.03.014

Harichandan B, Mandre NR (2022) Studies on the potential recovery of copper from low-grade mixed sulfide-oxide ore and optimization of the process parameters. Sep Sci Technol 57(5):719–732. https://doi.org/10.1080/01496395.2021.1933036

Javed U, Farooq R, Shehzad F, Khan Z (2018) Optimization of HNO3 leaching of copper from old AMD Athlon processors using response surface methodology. J Environ Manag 211:22–27. https://doi.org/10.1016/j.jenvman.2018.01.026

Katal R, Azizi A, Gharabaghi M (2020) Investigating the leaching behavior of copper from chalcopyrite concentrate in h2so4/cucl2 media. Iran J Mater Sci Eng 17(2):66–76

Kouhi RM, Ardejani FD, Tonkaboni SZS, Moghaddam MMJ, Butscher C, Taherdangkoo R (2024) A life cycle assessment study of acid mine drainage treatment using steel dust mineralization products. Mine Water and the Environment 43(4), 644–657. https://doi.org/10.1007/s10230-024-01005-0

Künkül A, Muhtar Kocakerim M, Yapici S, Demirbağ A (1994) Leaching kinetics of malachite in ammonia solutions. Int J Miner Process 41(3–4):167–182. https://doi.org/10.1016/0301-7516(94)90026-4

Levenspiel O (1998) Chemical reaction engineering. John Wiley & Sons, Hoboken, NJ, USA.

Li B, Wang XB, Wei YG, Wang H, Barati M (2018) Extraction of copper from copper and cadmium residues of zinc hydrometallurgy by oxidation acid leaching and cyclone electrowinning. Miner Eng 128:247–253. https://doi.org/10.1016/j.mineng.2018.09.007

Li Y, Kawashima N, Li J, Chandra AP, Gerson AR (2013) A review of the structure, and fundamental mechanisms and kinetics of the leaching of chalcopyrite. Adv Colloid Interface Sci 197:1–32. https://doi.org/10.1016/j.cis.2013.03.004

Liu ML, Wen JK, Tan GK, Liu GL, Wu B (2016) Experimental studies and pilot plant tests for acid leaching of low-grade copper oxide ores at the Tuwu Copper Mine. Hydrometallurgy 165:227–232. https://doi.org/10.1016/j.hydromet.2016.04.009

Mahmoudi Kouhi R, Jebrailvand Moghaddam MM, Rafie SF, Maghsoudy S, Doulati Ardejani F, Butscher C, Taherdangkoo R (2024) A quantitative framework for measuring sustainable development

goals in mining operations. Discov Sustain 5(1):313. https://doi.org/10.1007/s43621-024-00486-x

Mohanraj GT, Rahman MR, Arya SB, Barman R, Krishnendu P, Singh Meena S (2022) Characterization study and recovery of copper from low grade copper ore through hydrometallurgical route. Adv Powder Technol 33(1):103382. https://doi.org/10.1016/j.apt.2021.12.001

Montgomery DC (2001) Design and analysis of experiments. John Wiley & Sons Inc, New York

Rawlings DE, Johnson DB (2007) The microbiology of biomining: Development and optimization of mineral-oxidizing microbial consortia. Microbiology 153(2):315–324. https://doi.org/10.1099/mic.0.2006/001206-0

Schlesinger ME, Sole KC, Davenport WG, Flores GRA (2021) Extractive metallurgy of copper. Elsevier, Amsterdam, Netherland

Shi GC, Liao YL, Su BW, Zhang Y, Wang W, Xi JJ (2020) Kinetics of copper extraction from copper smelting slag by pressure oxidative leaching with sulfuric acid. Sep Purif Technol 241:116699. https://doi.org/10.1016/j.seppur.2020.116699

Sun XL, Chen BZ, Yang XY, Liu YY (2009) Technological conditions and kinetics of leaching copper from complex copper oxide ore. J Cent South Univ Technol 16(6):936–941. https://doi.org/10.1007/s11771-009-0156-6

Taherdangkoo R, Meng T, Amar MN, Sun YT, Sadighi A, Butscher C (2022) Modeling solubility of anhydrite and gypsum in aqueous solutions: Implications for swelling of clay-sulfate rocks. Rock Mech Rock Eng 55(7):4391–4402. https://doi.org/10.1007/s00603-022-02872-1

Tan QY, Deng C, Li JH (2017) Effects of mechanical activation on the kinetics of terbium leaching from waste phosphors using hydrochloric acid. J Rare Earths 35(4):398–405. https://doi.org/10.1016/S1002-0721(17)60925-6

Tanda BC, Eksteen JJ, Oraby EA, O'Connor GM (2019) The kinetics of chalcopyrite leaching in alkaline glycine/glycinate solutions. Miner Eng 135:118–128. https://doi.org/10.1016/j.mineng.2019.02.035

Wadsworth ME, Sohn HY (1979) Rate processes of extractive metallurgy. Plenum Press, New York.

Watling HR (2006) The bioleaching of sulphide minerals with emphasis on copper sulphides: A review. Hydrometallurgy 84(1–2):81–108. https://doi.org/10.1016/j.hydromet.2006.05.001

Xing YX, Liu Q, Hu R, Gu HB, Taherdangkoo R, Ptak T (2024) Global sensitivity analysis of water level response to harmonic aquifer disturbances through a Monte-Carlo based surrogate model with random forest algorithm. J Hydrol 641:131775. https://doi.org/10.1016/j.jhydrol.2024.131775